Structural Features and Electrochemical Properties of *ansa*-Ferrocenes with Pyrazabole Bridges†

Eberhardt Herdtweck,‡ Frieder Jäkle,‡ Giuliana Opromolla,§ Michael Spiegler,‡ Matthias Wagner,*,‡ and Piero Zanello*,§

Anorganisch-chemisches Institut der Technischen Universität München, Lichtenbergstrasse 4, D-85747 Garching, Germany, and Dipartimento di Chimica, Universitá di Siena, Pian dei Mantellini 44, 53100 Siena, Italy

Received August 21, 1996⊗

The stability of ferrocenophanes *ansa*-1,1′-Fc[B(R)(μ-pzR$^{\#}$)]$_2$ (**2**) with pyrazabole bridges depends to a large extent on the substitution pattern of boron (R) and pyrazole (R$^{\#}$). Cyclic voltammetry measurments on 17 derivatives of **2**, with R and R$^{\#}$ covering a wide spectrum of electronic features, revealed a pronounced influence of these substituents on the $E^{o\prime}_{0/+}$ values of the Fe(II)/Fe(III) redox couple. The electronic effects of R and R$^{\#}$ thus appear to be transmitted to a great degree along the pyrazabole framework. π donors R and electron acceptors R$^{\#}$ lead to a gradual *ansa*-bridge weakening and finally opening, if R = pyrrolidinyl and R$^{\#}$ = 3,5-CF$_3$ or 3,4,5-COOEt (NMR spectroscopy; X-ray crystal structure analyses of **2c** (R = Me; R$^{\#}$ = 3,4,5-H), **2d** (R = Me; pzR$^{\#}$ = indazolyl), **2n** (R = pyrrolidinyl; R$^{\#}$ = 3,4,5-H), **2p** (R = pyrrolidinyl; pzR$^{\#}$ = triazolyl)). Cyclic voltammetry indicates *ansa*-bridge opening to occur without major alterations of the charge density at boron. In the case of R = pyrrolidinyl there is evidence for negative hyperconjugation into the highly polar B−N(pyrazole) bonds. Oxidation of the central iron atom results in a contraction of the pyrazabole dimer (X-ray crystal structure analysis of **2c**$^+$).

Introduction

We have recently described the synthesis and chemical behavior of *ansa*-ferrocenes **Aa** with pyrazabole[1] bridges (Figure 1).[2,3] These studies are part of our ongoing attempts to realize novel structural motifs in organometallic chemistry by taking advantage of both the *facile formation* and the *reversible breaking and reforming* of boron−nitrogen(phosphorus) donor−acceptor bonds.

Our aim is to use such compounds as building blocks for the generation of redox-active host molecules (**B**; L-L, linker; Figure 2),[4,5] as well as for the synthesis of redox-responsive hemilabile ligands (**C**; D, NR_2, PR_2; Figure 2),[6] where the transition metal M* competes with the Lewis acidic boron centers for the electron lone pair at nitrogen or phosphorus.[7]

It is of prime importance in this context to achieve an equilibrium between the bridged structure **Aa** and the open-chain ferrocene **Ab** and to answer the question how it might be influenced *at will* (Figure 1). In the case of container molecules **B** made up of building blocks

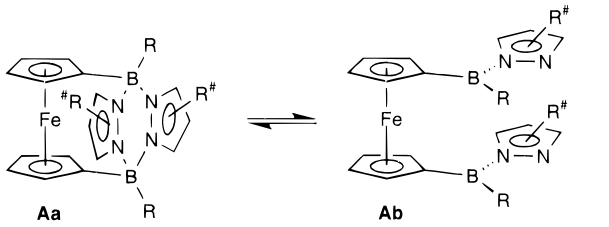

Figure 1. General representation of a ferrocenophane **A** with "switchable" pyrazabole bridge.

A, the rigidity of the whole molecular framework is obviously correlated with the stability of the pyrazabole dimer. To switch the *ansa*-bridges of the ferrocene fragments of **B** reversibly into an open-chain state would result in a more flexible macrocycle, which does not possess a well-defined cavity anymore. This could provide a means of smoothly releasing the guest from its complexed state, without destroying the host molecule. In the case of hemilabile ligands **C**, the stability of the ferrocenophane structure **Ca** and the formation constant of complexes **M*−Cb** are mutually dependent as well.

We have already shown the bridge stability of pyrazabole-bridged ferrocenophanes to be governed by electronic factors: While most substituents lead to ferrocenophane formation, the combination in the same molecule of a strongly π donating substituent at boron (e.g. R = pyrrolidinyl) with strongly π accepting groups at pyrazole (e.g. R$^{\#}$ = 3,4,5-COOEt[8]) results in an open-chain species even at low temperature.[3]

The purpose of this paper is to gain a more quantitative understanding about how the molecular structure

† Dedicated to Professor Walter Siebert on the occasion of his 60th birthday.

‡ Technische Universität München. Telefax (internat): +49-89-28913473. E-mail (internat): wagner@arthur.anorg.chemie.tu-muenchen.de.

§ Universitá di Siena. Telefax (internat): +39-577-280405. E-mail (internat): zanello@unisi.it.

⊗ Abstract published in *Advance ACS Abstracts,* November 15, 1996.

(1) Trofimenko, S. *J. Am. Chem. Soc.* **1967**, *89*, 4948−4952.

(2) Jäkle, F.; Priermeier, T.; Wagner, M. *J. Chem. Soc., Chem. Commun.* **1995**, 1765−1766.

(3) Jäkle, F.; Priermeier, T.; Wagner, M. *Organometallics* **1996**, *15*, 2033−2040.

(4) Beer, P. D.; Tite, E. L.; Drew, M. G. B.; Ibbotson, A. *J. Chem. Soc., Dalton Trans.* **1990**, 2543−2550.

(5) Jäkle, F.; Wagner, M. Unpublished results.

(6) Bader, A.; Lindner, E. *Coord. Chem. Rev.* **1991**, *108*, 27−110.

(7) Jäkle, F.; Mattner, M.; Priermeier, T.; Wagner, M. *J. Organomet. Chem.* **1995**, *502*, 123−130.

(8) The numbering of the *ansa*-bridges in compounds **2** follows the common numbering scheme for the parent heterocycles.

S0276-7333(96)00722-4 CCC: $12.00

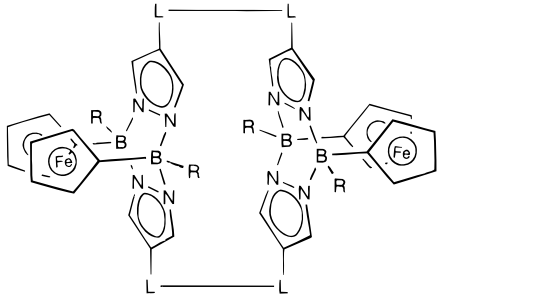

B

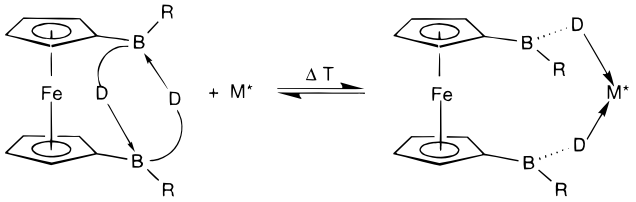

Ca M*-Cb

Figure 2. General representation of a redox-active container molecule made up of building blocks **A** (**B**; L-L, organic linker) and of a molecule of type **A** acting as hemilabile ligand to a transition metal complex M* (**C**; D, donor site NR_2, PR_2).

of ferrocenophanes **Aa** changes, (a) when the π donating ability of the substituent R is increased while the σ-donating ability of the pyrazolyl moiety is gradually decreased and (b) when the central iron atom is oxidized to the Fe(III) state. Moreover, we were interested to see to what extent the oxidation potential of iron varies with changes of the substitution pattern at boron and pyrazole.

Results and Discussion

A list of molecules **A** that have been chosen for investigation is given in Chart 1. Henceforth, individual derivatives of the general structure **A** are denoted **2a**−**s**.

Syntheses and Reactivities of Compounds 2. Ferrocenophanes **2d,i,m,o,p,r** (Chart 1) are obtained by stirring together 2 equiv of the respective pyrazole in toluene and a toluene solution of the appropriate derivative of **1** at low temperature. After the addition of neat triethylamine (2 equiv) and standard workup procedures, the crude products can readily be purified by recrystallization from di-*n*-butyl ether or toluene/hexane mixtures. This general reaction scheme is not suitable in the case of **2g**, because it leads to the formation of large amounts of ferrocene. Reasonably high yields of **2g** are obtained from **1b** and lithium 3,5-bis(trifluoromethyl)pyrazolide in toluene.

The reaction of **1b** and 1,2,4-triazole/NEt_3 gave an orange precipitate, which was only sparingly soluble in all common organic solvents. Bearing in mind that the nitrogen atom N4 is the most basic site of 1-*H*-1,2,4-triazole,[9] it is reasonable to assume that coordination polymers linked by *inter*molecular N4−B donor−acceptor bonds may be formed under these conditions (kinetic product control). When the Lewis acidity of the boron centers of **1** is decreased by substitution with π donor

(9) Katritzky, A. R., Rees, C. W., Eds. *Comprehensive Heterocyclic Chemistry*; Pergamon Press: Oxford, U.K., 1984.

Chart 1. Survey of Compounds 1 and 2

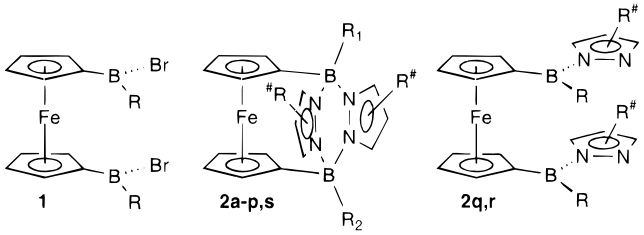

1 2a-p,s 2q,r

1	R
a	Br
b	Me
c	OEt
d	NC_4H_8

2	$R_1 = R_2 = R$	$pzR^{\#}$
a[a]	Br	3,4,5-H
b[a]	Br	3,5-Me; 4-H
c[a]	Me	3,4,5-H
d[b]	Me	indazolyl
e[c]	Me	3,5-Me; 4-Br
f[a]	Me	3,4,5-COOEt
g[b]	Me	3,5-CF_3; 4-H
h[a]	OEt	3,4,5-H
i[b]	OEt	triazolyl
j[a]	OEt	3,4,5-COOEt
k[a]	$N_2C_3H_3$	3,4,5-H
l[b]	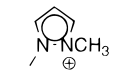	3,4,5-H
m[b]	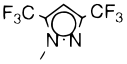	3,5-CF_3; 4-H
n[a]	NC_4H_8	3,4,5-H
o[b]	NC_4H_8	indazolyl
p[b]	NC_4H_8	triazolyl
q[a]	NC_4H_8	3,4,5-COOEt
r[b]	NC_4H_8	3,5-CF_3; 4-H
	R1 ≠ R2	
s[b]	pyrrolidinyl triazolyl	triazolyl

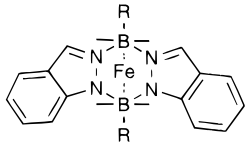

meso-**2d,o**

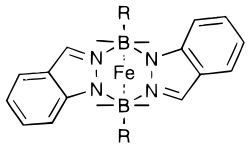

rac-**2d,o** (one enantiomer)

[a] See ref 3. [b] This work. [c] See ref 2.

groups (e.g. OEt, **1c**; pyrrolidinyl, NC_4H_8, **1d**), the rate of N−B adduct formation can be expected to drop, which should lead to thermodynamic product control and thus to the formation of the triazolyl analogue of **2h,n**. This view is confirmed by the successful synthesis of ferrocenophanes **2i,p**. However, the yield of **2i** is still only modest (45%) due to the formation of a significant amount of other (polymeric) products. A different kind of byproduct, which results from a transamination reaction, is observed in the case of **2p**, where the rather acidic triazole can displace one of the more basic pyrrolidinyl groups to give the first example of a ferrocenophane **Aa** bearing two different substituents R_1, R_2 at the two boron centers (**2s**; Chart 1). When analytically pure **2p** was dissolved in di-*n*-butyl ether and kept at reflux temperature for 1 h, the crystalline material formed upon cooling consisted entirely of **2s**. The compound is most likely formed after thermal *ansa*-bridge opening as a reaction product of open-chain **2p**.

When exposed to air, **2p** decomposes slowly even in the solid state, whereas the pyrazolyl analogue **2n** is much more stable under the same conditions. These cited observations indicate the interannular B−N bonds of **2p** to be weakened as a result of the negative inductive effect of the third nitrogen atom. The same is true for **2r** with its strongly electron-withdrawing CF_3

Scheme 1. *ansa*-Bridge Opening in 2i upon Methylation of Nitrogens N4[a]

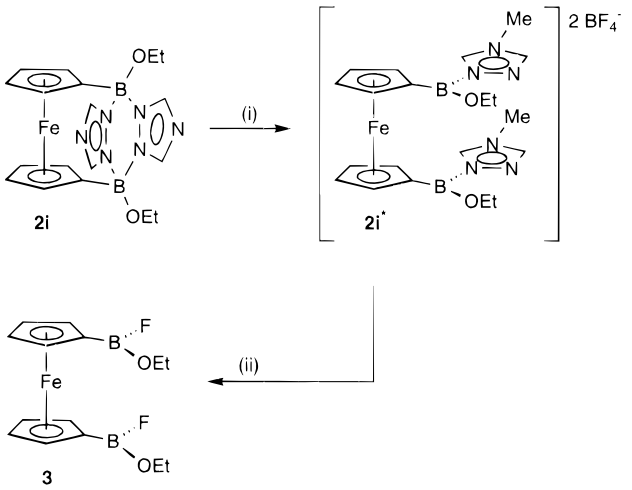

[a]Key: (i) $+2Me_3O^+BF_4^-$; (ii) $-2BF_3$·tzMe.

substituents. This compound has to be kept strictly under an inert-gas atmosphere and is therefore very similar to **2q**, in that those two molecules are by far the most sensitive derivatives of **A**.

In an attempt to further decrease the Lewis basicity of its triazolyl moiety by methylating both nitrogen atoms N4, **2i** was treated with Meerwein's salt ($Me_3O^+BF_4^-$). The reaction led to the complete destruction of the *ansa*-bridge and gave 1,1′-bis(ethoxyfluoroboryl)ferrocene, **3**, as the only characterizable ferrocene-containing species. This result provides good evidence for the existence of an unstable open-chain intermediate **2i*** and, thus, indicates a possible way to induce *ansa*-bridge opening by employing Lewis acidic additives (Scheme 1).

Due to the oily nature of the air-sensitive compound **3**, a satisfactory elemental analysis was not obtained. We have therefore proven the proposed structure of **3** by synthesizing this compound also via a different route, starting from **1c** and 2 equiv of thallium(I) fluoride in toluene. The ^1H, ^{13}C, and ^{11}B NMR spectra of both reaction products are identical.

Spectroscopic Properties of Compounds 2. The question whether a particular derivative **2** adopts a bridged or an open-chain conformation can easily be answered by NMR spectroscopy. With the exception of **2d,o,q,r,s** all compounds exhibit two resonances for the ferrocene fragment, both in the ^1H and in the ^{13}C NMR spectra. One of the two proton signals appears at remarkably high field, which is a characteristic feature of ferrocenes with pyrazabole bridges.[3] The carbon atoms $C_{3,5}$[8] in the pyrazolyl rings, as well as the substituents attached to these atoms, give rise to only one set of signals, thereby proving both positions to be magnetically equivalent. This again is indicative for a ferrocenophane structure with its two orthogonal planes of symmetry. Despite of their enhanced sensitivity toward air and moisture, neither **2j** nor **2p** shows any detectable concentration of an open-chain conformer at temperatures up to 100 °C ([D_8]toluene solution).

The magnetic equivalence of positions 3 and 5 of the pyrazolyl rings is no longer maintained in **2q,r**, which also show a complicated pattern of ferrocene resonances. In **2r** most NMR signals are split into a set of two resonances, which coalesce in the temperature range between +50 and +90 °C and thus indicate rotational hindrance due to steric congestion. Both the reduced molecular symmetry and the dynamic phenomena apparent in the NMR spectra of **2q,r** point to an open-chain structure of these molecules. These findings suggest that not only π acceptors at pyrazole but σ acceptors as well have a destabilizing effect on the pyrazabole bridge. This destabilization is strong enough to prevent the formation of *ansa*-**2q,r** in solution, even at temperatures as low as −80 °C (^1H, ^{13}C, ^{11}B NMR spectroscopy). The same is true for **2q** in the solid state: Apart from the expected line broadening, its ^{13}C solid-state NMR spectrum is almost identical with the one in solution, which excludes any presence of *ansa*-**2q**.

The indazole derivative **2d** was investigated, because some of the pyrazolyl-bridged derivatives of **2** show a second oxidation wave in addition to that of the Fe(II)/Fe(III) couple, which appears at rather high potential and might be assigned to an electron removal from the pyrazabole fragment (see below). Extending the π system of the pyrazabole unit by using indazole rather than pyrazole should lower its oxidation potential and thus prove or disprove this assignment. **2d** was obtained as a mixture of its *rac* and *meso* forms (Chart 1). Both diastereomers can easily be distinguished and identified NMR spectroscopically, because *rac*-**2d** possesses a C_2-axis, whereas *meso*-**2d** possesses a mirror plane. The B−Me groups of the former are therefore magnetically equivalent, while in the latter two resonances for the methyl substituents are observed. Mutual assignments of ^1H and ^{13}C resonance signals are based on 2D heteronuclear shift correlations. Together with $^1H/^1H$ COSY and ^1H NOE difference spectra a complete assignment of all ^1H and ^{13}C NMR signals of both diastereomers was achieved. *meso*-**2d** was isolated in pure form by recrystallizing the mixture of *rac*/*meso*-**2d** from toluene. The reaction of the very Lewis acidic **1b** with indazole/NEt_3 gave a higher yield of *rac*-**2d** at low temperature (−78 °C, *rac*:*meso* = 6:4) but increasing amounts of the *meso*-diastereomer at higher reaction temperatures (−40 °C, *rac*:*meso* = 3:7). Crude **2o** always consisted of an equal proportion of *rac*- and *meso*-**2o** (*rac*:*meso* = 1:1), and the pyrazole-fused benzo ring did not exhibit a distinct directive effect in the formation of the pyrazabole bridge.

In **2l,m** two sets of signals are observed in the ^1H, ^{13}C, and ^{19}F (**2m**) NMR spectra. This phenomenon has to be attributed to a high rotational barrier around the exocyclic B−N bonds due to steric congestion, which results in two stable rotamers even at ambient temperature. Only the spectra of **2m** will be discussed in greater detail; however, similar arguments hold for **2l**. In the case of **2m**, one set of NMR resonances can easily be assigned to rotamer 2 (Chart 2).

The presence of four signals in the ferrocene region of the ^1H and ^{13}C NMR spectra, together with six signals for the CF_3 groups (^{19}F NMR spectrum), clearly indicates symmetry breaking, caused by two exocyclic pyrazolyl substituents with different orientations. The second set of signals has to belong to a more symmetrical rotamer, exhibiting only two signals for the ferrocene fragment and three signals for the CF_3 substituents. The ^{19}F NMR data of **2m** are particularly revealing. Pronounced fluorine−fluorine coupling is

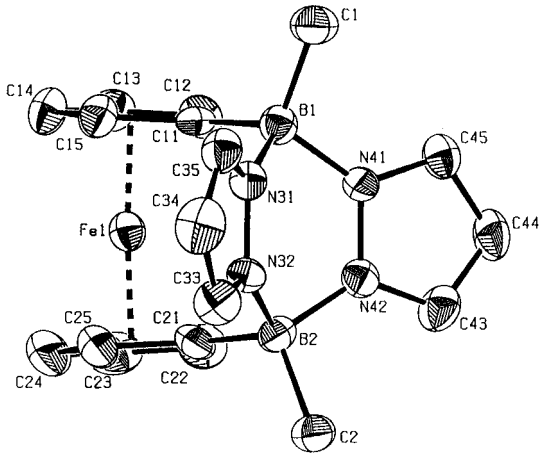

Figure 3. Platon plot of $\mathbf{2c}^+$ with counterion (BF_4^-) omitted. Thermal ellipsoids are drawn at the 50% probability level.

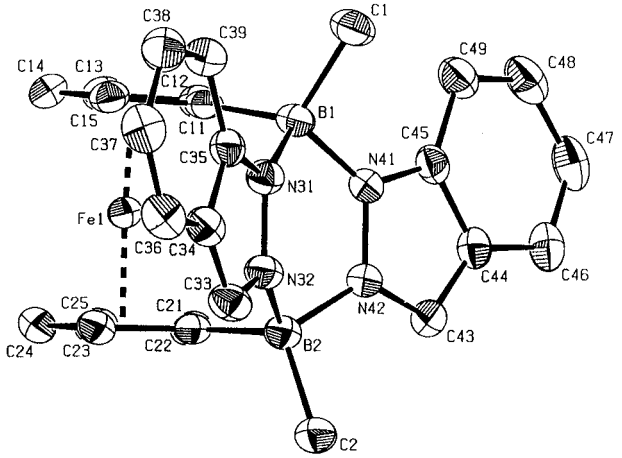

Figure 4. Platon plot of *meso*-**2d**. Thermal ellipsoids are drawn at the 50% probability level.

Chart 2. Three Possible Rotamers of Sterically Crowded 2m

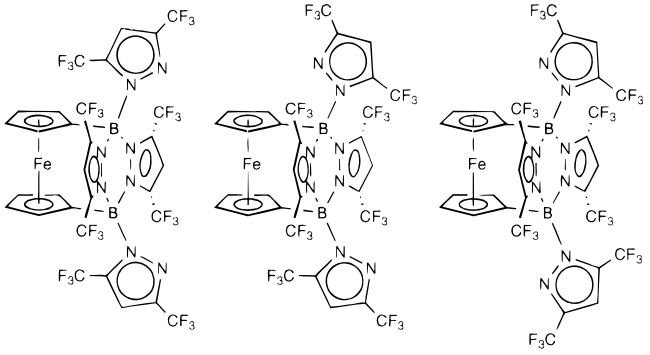

2m (Rotamer 1) **2m** (Rotamer 2) **2m** (Rotamer 3)

observed (J(FF) = 10 Hz), even though all fluorine atoms belonging to different CF_3 substituents are separated by at least 6 bonds. A through-bond coupling mechanism is thus unlikely, and we therefore confidently assume fluorine−fluorine coupling to occur via a through-space mechanism.[10] This mechanism is known to be particularly efficient when close nonbonding F···F interactions are present in a rigid molecular framework. Both conditions are met by the ferrocenophane derivative **2m**. Consequently, three signals with integral ratios of 1 (singlet):1 (septet):2 (quartet) may be assigned either to rotamer 1 or 3, where only one of the two different exocyclic CF_3 groups couples to two endocyclic CF_3 groups, thereby generating the signal pattern cited above. An analogous interpretation of the ^{19}F NMR data is possible for the less symmetric rotamer 2 (see Experimental Section). All data available for **2m** are in accord both with rotamer 1 and with rotamer 3, and thus the precise structure of this species is still somewhat ambiguous. However, NOE difference

(10) Emsley, J. W.; Phillips, L.; Wray, V. *Fluorine Coupling Constants*; Pergamon Press: Oxford, U.K., 1977.

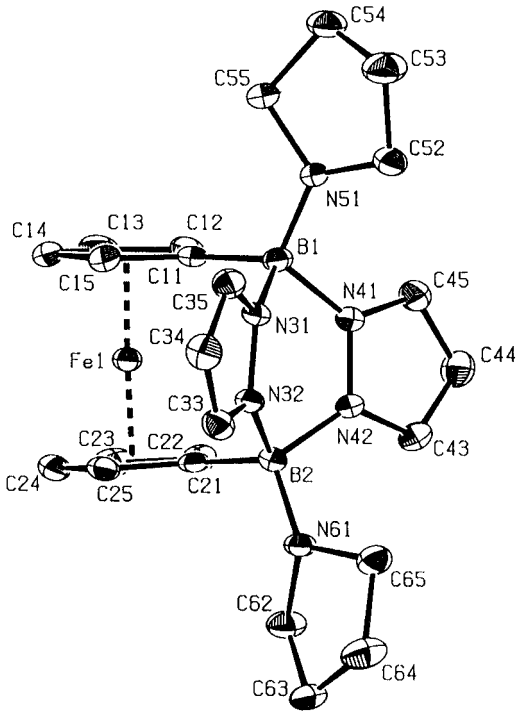

Figure 5. Platon plot of **2n**. Thermal ellipsoids are drawn at the 50% probability level.

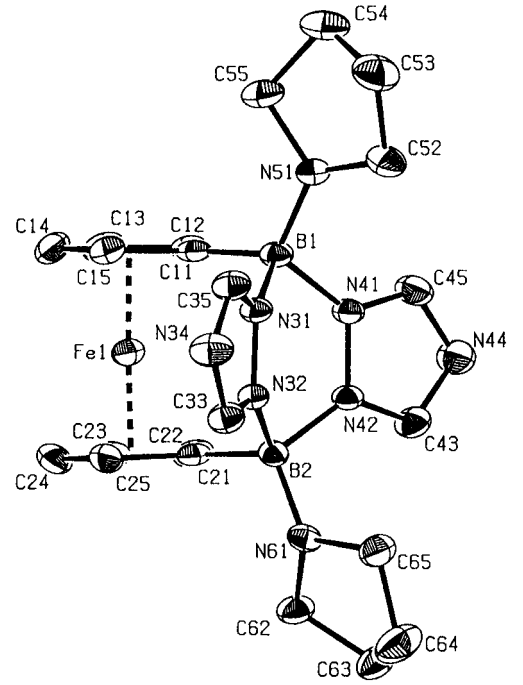

Figure 6. Platon plot of **2p**. Thermal ellipsoids are drawn at the 50% probability level.

Table 1. Summary of Crystallographic Data for Ferrocenophanes $2c^+$−2p

compd	$2c^+$	*meso*-2d	2n	2p
formula	$C_{18}H_{20}B_3F_4FeN_4$	$C_{26}H_{24}B_2FeN_4$	$C_{24}H_{30}B_2FeN_6$	$C_{22}H_{28}B_2FeN_8$
fw	456.66	469.97	480.01	481.99
cryst dimen, mm	0.43 × 0.25 × 0.25	0.89 × 0.51 × 0.43	0.43 × 0.41 × 0.25	0.38 × 0.38 × 0.20
cryst syst	monoclinic	triclinic	monoclinic	monoclinic
space group	*Ia*	$P\bar{1}$	$P2_1/n$	$P2_1/n$
temp, K	193	193	193	193
a, Å	14.921(2)	10.097(2)	10.637(3)	8.690(1)
b, Å	24.633(2)	10.730(2)	16.307(2)	22.365(2)
c, Å	22.874(3)	10.800(2)	13.274(4)	12.407(1)
α, deg	90	65.70(2)	90	90
β, deg	102.19(1)	86.93(1)	97.09(1)	108.88(1)
γ, deg	90	80.62(1)	90	90
V, Å^3	8218(2)	1052.0(4)	2284.9(10)	2281.6(4)
D_{calc}, g·cm^{-3}	1.476	1.484	1.395	1.403
Z	16	2	4	4
radiation, Å	Mo Kα, 0.710 73	Mo Kα, 0.710 73	Mo Kα, 0.710 73	Mo Kα, 0.710 73
no. of tot. reflns	45 311	4520	5280	4088
no. of uniq reflns	12 772	4098	4024	3918
no. of obsd reflns	12 770	4098	4024	3918
no. of params	1075	394	418	411
μ, cm^{-1}	7.8	7.4	6.9	6.9
final $R1$ [a]	0.050	0.031	0.049	0.050
final w$R2$ [b]	0.116	0.077	0.089	0.094
GOF[c]	1.082	1.076	1.077	1.065

[a] $R1 = \Sigma(||F_o| - |F_c||)/\Sigma|F_o|$. [b] $wR2 = [\Sigma w (F_o^2 - F_c^2)^2/\Sigma w (F_o^2)^2]^{1/2}$. [c] $GOF = [\Sigma w (F_o^2 - F_c^2)^2/(NO - NV)]^{1/2}$.

spectra of a ferrocenophane closely related to **2m**, which bears CH_3 rather than CF_3 substituents, show a positive NOE effect between one of the two exocyclic methyl groups and the ferrocene resonances.[11] These findings are in better agreement with rotamer 1 than with rotamer 3.

Paramagnetic NMR spectra were recorded for $\mathbf{2c}^+$, which was obtained upon treatment of **2c** with $AgBF_4$. As expected, the line broadening, as well as the paramagnetic shifts, are by far most pronounced for the ferrocene resonances. However, it is noteworthy that not only the boron nuclei but also the methyl groups and even the pyrazolyl rings do show significant paramagnetic shifts. A more detailed study on the paramagnetic NMR spectra of compounds $\mathbf{2}^+$ and on the spin density distribution in these ferrocenium cations is currently in progress.

Molecular Structures. Compounds $\mathbf{2c}^+$, **2c**,[3] *meso*-**2d**, **2n**, and **2p** were chosen for a comparison of their solid-state structures, because they differ significantly in their electronic properties but vary only little as far as their steric features are concerned.

Deep blue $\mathbf{2c}^+$ crystallizes from CH_2Cl_2/hexane in the monoclinic acentric space group *Ia* with four crystallographically independent molecules in the asymmetric unit ($\mathbf{2c}^+$, $\mathbf{2c}^+\mathbf{A}$, $\mathbf{2c}^+\mathbf{B}$, $\mathbf{2c}^+\mathbf{C}$). Since these molecules possess very similar geometries, only one of them ($\mathbf{2c}^+$) is given below (Figure 3). X-ray-quality crystals of *meso*-**2d** (triclinic, $P\bar{1}$), **2n** (monoclinic, $P2_1/n$), and **2p** (monoclinic, $P2_1/n$) were grown from toluene, di-*n*-butyl ether, and toluene/hexane, respectively (Figures 4−6, Tables 1−4). The complete set of structure data of $\mathbf{2c}^+$, *meso*-**2d**, **2n**, and **2p** is available on request.[12]

B−N donor−acceptor bonds are weaker than the isoelectronic covalent C−C links and thus show greater variations of their individual bond lengths. For a comparison of the molecular structures of $\mathbf{2c}^+$, **2c**, *meso*-**2d**, **2n**, and **2p**, we will therefore use the mean values of all chemically equivalent bonds in the respective asymmetric units (Table 4). Standard deviations of these mean values are not given, because the number of crystallographically nonequivalent molecules that contribute to each mean value are not the same in the series $\mathbf{2c}^+$ to **2p**.

Table 2. Selected Bond Lengths (Å) of Molecules $2c^+$, *meso*-2d, 2n, and 2p [a]$2c^+$, *meso*-2d, X = C(1), Y = C(2); 2n,p, X = N(51), Y = N(61)

	$2c^+$	*meso*-2d	2n	2p
B(1)−X[a]	1.597(7)	1.619(3)	1.476(4)	1.479(4)
B(1)−C(11)	1.603(6)	1.606(3)	1.590(5)	1.588(4)
B(1)−N(31)	1.575(6)	1.593(3)	1.608(3)	1.615(4)
B(1)−N(41)	1.576(6)	1.595(3)	1.601(4)	1.602(3)
N(31)−N(32)	1.363(4)	1.363(2)	1.355(3)	1.366(3)
B(2)−Y[a]	1.603(6)	1.603(3)	1.475(4)	1.481(4)
B(2)−C(21)	1.599(7)	1.606(3)	1.598(5)	1.591(4)
B(2)−N(32)	1.565(5)	1.569(3)	1.594(4)	1.594(3)
B(2)−N(42)	1.574(6)	1.573(3)	1.607(4)	1.622(4)
N(41)−N(42)	1.362(4)	1.362(2)	1.356(3)	1.363(3)

The mean values (C−C) of the C(13)−C(14) and C(23)−C(24) bonds of molecules $\mathbf{2c}^+$ to **2p** do serve as an internal standard for the estimation of bond length variations arising from the inherent analytical inaccuracy of the crystal structure determinations.

An important feature of the solid state structures of $\mathbf{2c}^+$ to **2p** is the gradual increase of the mean B−N(pz) bond lengths: $\mathbf{2c}^+$ < **2c** < *meso*-**2d** < **2n** < **2p** . Even though the differences between each pair of neighbors are small, a general trend is evident and the overall difference $\Delta_{B-N(pz)}(\mathbf{2p}-\mathbf{2c}^+) = 0.040$ Å is undoubtedly significant (B−N(pz): mean values of all B−N(pz) bonds in the asymmetric units of $\mathbf{2c}^+$ and **2p**). In contrast to $\Delta_{B-N(pz)}$, the Δ_{C-C} values of $\mathbf{2c}^+$ to **2p** are smaller than 0.007 Å and show a random distribution (C−C: mean values of all C(13)−C(14)/C(23)−C(24) bonds in the asymmetric units of $\mathbf{2c}^+$ to **2p**). The trend in B−N(pz) bond length variations is further reflected by the cyclopentadienyl tilt angles of the ferrocenyl fragments. A

(11) Gmeinwieser, T.; Wagner, M. Unpublished results.

(12) Further details of the crystal structure investigations are available on request from the Fachinformationszentrum Karlsruhe, Gesellschaft für wissenschaftlich-technische Information mbH, D-76344 Eggenstein-Leopoldshafen, Germany, on quoting the depository numbers CSD 406029 ($\mathbf{2c}^+$), CSD 406028 (*meso*-**2d**), CSD 406027 (**2n**), and CSD 406026 (**2p**), the names of the authors, and the literature citation.

Table 3. Selected Angles (deg) and Angles between Planes (deg) of Molecules $2c^+$, *meso*-2d, 2n, and 2p

	$2c^+$	*meso*-**2d**	**2n**[b]	**2p**[c]
X−B(1)−C(11)[a]	112.7(3)	117.3(2)	113.8(2)	115.2(2)
X−B(1)−N(31)[a]	110.6(3)	108.9(2)	112.5(2)	111.5(2)
X−B(1)−N(41)[a]	110.6(4)	107.5(2)	109.7(2)	109.4(2)
C(11)−B(1)−N(31)	109.7(3)	108.1(2)	107.7(2)	108.5(2)
C(11)−B(1)−N(41)	110.0(3)	108.2(2)	110.9(2)	110.8(2)
N(31)−B(1)−N(41)	102.7(3)	106.3(1)	101.6(2)	100.4(2)
Y−B(2)−C(21)[a]	112.2(4)	115.4(2)	113.5(2)	114.8(2)
Y−B(2)−N(32)[a]	110.2(3)	109.1(2)	109.0(2)	110.2(2)
Y−B(2)−N(42)[a]	109.4(4)	110.5(2)	113.1(2)	111.9(2)
C(21)−B(2)−N(32)	110.8(3)	109.2(2)	111.1(2)	110.3(2)
C(21)−B(2)−N(42)	110.2(3)	107.6(2)	107.9(2)	108.0(2)
N(32)−B(2)−N(42)	103.8(3)	104.5(1)	101.7(2)	100.7(2)
C(11)−C(15)//C(21)−C(25)	7.4	3.4	3.2	2.7
N(31)−C(35)//N(41)−C(45)	45.1	23.9	32.2	35.2
B(1)N(31)N(32)B(2)//B(1)N(41)N(42)B(2)	44.1	39.4	44.5	45.1
B(1)N(31)N(41)//N(31)N(32)N(41)N(42)	31.2	22.6	30.2	30.1
B(2)N(32)N(42)//N(31)N(32)N(41)N(42)	30.3	33.6	30.0	29.8

[a] $2c^+$, *meso*-**2d**, X = C(1), Y = C(2); **2n**,**p**, X = N(51), Y = N(61). [b] Sum of angles around N(51) [N(61)]: 356.0° [354.5°]. [c] Sum of angles around N(51) [N(61)]: 356.4° [352.8°].

Table 4. Mean Values of Selected Bond Lengths (Å) of Molecules $2c^+$, 2c, *meso*-2d, 2n, and 2p

	$2c^+$	2c	*meso*-**2d**	2n	2p
B−X[a]	1.600	1.600	1.611	1.476	1.480
B−C(Cp)	1.608	1.593	1.606	1.594	1.591
B−N(pz)	1.569	1.578	1.583	1.603	1.609
N(pz)−N(pz)	1.363	1.360	1.363	1.356	1.364
C−C[b]	1.413	1.419	1.418	1.412	1.418

[a] $2c^+$, **2c**, *meso*-**2d**, X = C(Me); **2n**,**p**, X = N(pyrrolidinyl). [b] Mean value of all C(13)−C(14)/C(23)−C(24) bonds in the asymmetric unit.

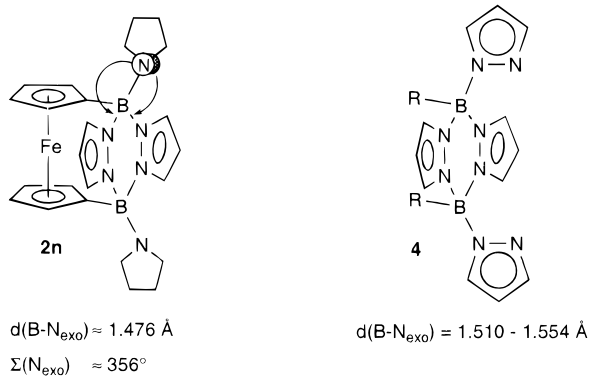

Figure 7. Structural features indicating negative N−B hyperconjugation in **2n** (R = H, Et, Ph, pz).

continuous decrease of this angle from 7.5° (mean value) in $2c^+$ to 2.7° in **2p** is observed, as the B−N(pz) bond lengths are increasing.

If we look at the fragment $C_4H_8N-B(sp^3)$, the sum of angles around N(51) [N(61)] is 356.0° [354.5°] in **2n** and 356.4° [352.8°] in **2p**. These values are considerably larger than in the analogous compounds $C_4H_8N-C(sp^3)$, where the sum of angles around nitrogen normally does not exceed 335°.[13] The B−N(51) [B−N(61)] bond lengths are 1.476(4) [1.475(4)] and 1.479(4) Å [1.481(4) Å] in **2n**,**p**, respectively. In contrast, the exocyclic B−N(pz) bond lengths in pyrazaboles **4** with pyrazolyl substituents at boron (Figure 7) fall in the range 1.510−1.554 Å.[14−17] If we bear in mind that the covalent radius of an sp^2 nitrogen atom in aromatic pyrazole is unlikely to be larger than that of a dialkylamido nitrogen atom, the reverse order of B−N bond lengths could be expected, if those links were pure single bonds. We therefore conclude that the short B−N(pyrrolidine) bonds in **2n**,**p**, together with the pronounced flattening of the nitrogen atoms N(51) and N(61) is indicative for some degree of π bonding in these molecules. Since pyrazoles are considerably weaker π donors than pyrrolidines, exocyclic B−N(pz) bonds in pyrazolyl-substituted pyrazaboles show larger bond lengths.

The pyrrolidine rings are located in the plane spanned by the atoms B(1), Fe, and B(2), thereby minimizing nonbonding interactions with the bridging pyrazolyl rings. A hindered rotation around the B−N(pyrrolidine) bonds of **2n** is also apparent in solution. For example, broad signals are observed for the pyrrolidine protons in the ^{1}H NMR spectra of **2n**, which split into a set of four resonances at −20 °C. This preferred conformation of the amido groups facilitates a negative hyperconjugative interaction[18−21] between the pyrrolidine electron lone pair (which has essentially p character) and the two antibonding orbitals of the adjacent highly polar B−N(pz) bonds (Figure 7). A mechanism of boron−pyrrolidine π interaction is thus provided, which could account for the short B−N(pyrrolidine) and large B−N(pz) bonds.

Electrochemical Studies of *ansa*-Ferrocenes. The substituents attached to boron or pyrazole in compounds **2** cover a wide spectrum of electronic features, ranging from strongly electron-releasing to strongly electron-withdrawing effects. Thus, exploring the redox potentials of **2a**−**p** provides an opportunity to monitor the transmission of these electronic effects along the pyrazabole framework. One major question is to which extent the electronic influence of substitu-

(13) Allen, F. H.; Kennard, O.; Taylor, R. *Acc. Chem. Res.* **1983**, *16*, 146−153.
(14) Alcock, N. W.; Sawyer, J. F. *Acta Crystallogr.* **1974**, *B30*, 2899−2901.
(15) Niedenzu, K.; Nöth, H. *Chem. Ber.* **1983**, *116*, 1132−1153.
(16) Brock, C. P.; Niedenzu, K.; Hanecker, E.; Nöth, H. *Acta Crystallogr.* **1985**, *C41*, 1458−1463.
(17) Bielawski, J.; Das, M. K.; Hanecker, E.; Niedenzu, K.; Nöth, H. *Inorg. Chem.* **1986**, *25*, 4623−4628.
(18) Epiotis, N. D.; Cherry, W. R.; Shaik, S.; Yates, R. L.; Bernardi, F. *Top. Current Chem.* **1977**, *70*, 177ff.
(19) Farnham, W. B.; Smart, B. E.; Middleton, W. J.; Calabrese, J. C.; Dixon, D. A. *J. Am. Chem. Soc.* **1985**, *107*, 4565−4567.
(20) Rahman, M. M.; Lemal, D. M.; Dailey, W. P. *J. Am. Chem. Soc.* **1988**, *110*, 1964−1966.
(21) Salzner, U.; Schleyer, P. v. R. *J. Am. Chem. Soc.* **1993**, *115*, 10231−10236.

ents R_1, R_2, and $R^{\#}$ on iron is attenuated by the ligating tetracoordinate boron atoms, as compared to sp^3 carbon atoms in the same place.[22] Another problem of interest is whether the inductive effects of $R_{1,2}$ are transmitted predominantly or whether resonance effects are also likely to play a significant role. This problem is closely connected with questions related to the mechanism of *ansa*-bridge opening and closing: A strong π donor like pyrrolidine may either actively weaken the B−N(pz) bonds by hyperconjugation and charge delocalization into antibonding B−N orbitals (see Molecular Structures) or just stabilize a three-coordinate boron center once it has been formed.

The cyclic voltammogram of complex **2c** in CH_2Cl_2 solution reveals an oxidation process at $E^{\circ\prime} = +0.13$ V. Controlled potential coulometry ($E_w = +0.5$ V) shows the anodic process to consume one electron per molecule. The blue solution (λ_{max} = 638 nm) resulting from exhaustive oxidation displays a cyclic voltammetric profile quite complementary to that of the original **2c**. Analysis[23] of the cyclic voltammograms with scan rates varying from 0.02 to 1.00 V s^{-1} shows that (a) the i_{pc}/i_{pa} ratio is constantly equal to 1, (b) the current function $i_{pa}/v^{1/2}$ remains constant, and (c) the peak-to-peak separation progressively increases from 70 mV at 0.02 V s^{-1} to 146 mV at 1.00 V s^{-1}. In spite of the deviation of this latter value from the constant value of 59 mV theoretically expected for an electrochemically reversible one-electron transfer, it must be noted that under the same experimental conditions the one-electron oxidation of ferrocene displays a similar trend in peak-to-peak separation. On this basis we confidently assume that the oxidation process **2c**/**2c**$^+$ involves an essentially reversible electron transfer, as proven by the synthesis and isolation of **2c**$^+$ as its BF_4^- salt. The electrochemical results confirm that only subtle structural reorganizations accompany the electron removal,[24] which agrees well with the previously discussed crystallographic data. The behavior discussed for complex **2c** is typical for all the *ansa*-bridged ferrocenes **2**; their relevant redox potentials are compiled in Table 5, together with related UV−visible spectroscopic data.

In most cases, the pyrazabole bridge makes the electron removal from the ferrocene fragments easier, compared to unsubstituted ferrocene. However, the wide range of substituents inserted on the different pyrazabole sites appreciably affects the location of the redox potentials. For instance, in CH_3CN solution a positive shift of 0.25 V takes place on passing from **2c** to **2a**. In addition, the presence of eight electron-withdrawing CF_3 groups in **2m** leads to a redox potential of the iron center 0.52 V higher than that of **2c** and still 0.29 V higher than that of the FcH/FcH$^+$ couple (Fc = Fe(η^5-C_5H_4)(η^5-C_5H_5); Table 5). The fact that in all cases the exhaustively oxidized solutions assume a blue color gives evidence for the iron-centered character of the HOMO level.

Recent electrochemical studies by Silva et al. have indicated that "the oxidation potential of ferrocene derivatives may be used as a probe in the study of the electronic properties of substituent groups, since their effects are transmitted through the carbocyclic ring to the iron redox active center".[22] The following discussion of electrochemical results is based on the assumption of a direct interdependence between the electron density at boron and the electron density at iron, as manifested by its redox potential. Because of the lack of the Hammett constants of substituents such as pyrazolyl, indazolyl, pyrrolidinyl and triazolyl,[25] and in spite of the conceivable hypothesis that a linear relationship should hold within each class of compounds having either the same substituent at boron or the same substituents at the pyrazole rings, any attempt of a quantitative correlation among complexes **2a**−**p** was unsuccessful.

Table 5. Electrochemical Characteristics for the Oxidation Process Exhibited by *ansa*-Bridged Complexes 2a−p

2	$E^{\circ\prime}_{0/+}$ (V)	ΔE_p[a] (mV)	λ_{max}[b] (nm)
a	+0.43[c]/+0.40[d,e]	70[c]/60[d]	640[c]
b	+0.30[c]/+0.20[d]	64[c]/71[d]	631[c]
c	+0.13[c]/+0.15[d]	76[c]/66[d]	638[c]
d	+0.16[c]/+0.15[d,f]	88[c]/66[d,f]	638[c]
e	+0.15[c]/+0.16[d,f]	78[c]/73[d,f]	636[c]
f	+0.24[c]/+0.28[d]	78[c]/86[d,f]	634[c]
g	+0.45[c]/+0.45[d,f]	66[c]/70[d]	*g*
h	+0.25[c]/+0.26[d]	84[c]/72[d]	647[c]
i	+0.38[c]/+0.35[d]	80[c]/76[d]	632[c]
j	+0.38[c]/+0.40[d]	76[c]/70[d]	622[c]
k	+0.40[c]/+0.39[d]	74[c]/68[d]	634[c]
l	-[c,f]/+0.61[d]	-[c,f]/66[d]	635[d]
m	+0.63[c]/+0.67[d]	94[c]/74[d]	631[c]
n	+0.14[c]/+0.21[d]	86[c]/82[d]	635[c]
p	+0.29[c]/+0.22[d]	75[c]/80[d]	*g*
FcH	+0.39[c]/+0.38[d]	90[c]/70[d]	620[c]

[a] Measured at 0.1 V s^{-1}. [b] Referred to the oxidized species. [c] Measured in CH_2Cl_2. [d] Measured in CH_3CN. [e] Unstable species. [f] Poorly soluble. [g] Extremely air sensitive.

Nevertheless, the following semiquantitative conclusions may be drawn: When compounds with different substituents R at boron, but with the same bridging pyrazolyl derivative ($R^{\#}$ = 3,4,5-H) are compared, the following order of decreasing electron density at iron is observed in CH_3CN solution (Table 5): **2c** (R = Me; $E^{\circ\prime}_{0/+} = +0.15$ V) > **2n** (NC_4H_8; +0.21 V) > **2h** (OEt; +0.26 V) > **2k** ($N_2C_3H_3$; +0.39 V) ≈ **2a** (Br; +0.40 V). It is apparent that this observation cannot be the result of inductive substituent effects only, because in this case a completely different order of **2c** > **2a** > **2n** > **2k** ≈ **2h** would have to be expected. The electrochemical findings thus give further support to the hypothesis of a marked hyperconjugative π interaction between substituent lone pairs and the boron centers as already deduced from the X-ray structure data. When the change is made from R = Me to R = NC_4H_8, the increased B-R σ bond polarity is almost completely offset by nitrogen lone pair donation. The pyrazolyl derivative **2k** possesses a boron-bound nitrogen center of similar electronegativity compared to the substituents in **2h,n**. However, delocalization of its electron lone pair results in weaker B−N π donation and thus in a decrease of electron density at boron, as monitored by the higher oxidation potential of the iron center (**2k**: $E^{\circ\prime}_{0/+} = +0.39$ V; CH_3CN). When both nitrogen centers of the exocyclic pyrazolyl substituents in **2k** are methylated using Meerwein's salt, the

(22) Silva, M. E. N. P. R. A.; Pombeiro, A. J. L.; da Silva, J. J. R. F.; Herrmann, R.; Deus, N.; Castilho, T. J.; Silva, M. F. C. G. *J. Organomet.Chem.* **1991**, *421*, 75−90.
(23) Brown, E. R.; Sandifer, J. In *Physical Methods in Chemistry. Electrochemical Methods*; Rossiter, B. W., Hamilton, J. F., Eds.; Wiley: New York, 1986.
(24) Zanello, P. *Struct. Bonding* **1992**, *79*, 101−214.
(25) Hansch, C.; Leo, A.; Taft, R. W. *Chem. Rev.* **1991**, *91*, 165−195.

dication **2l** is obtained in a clean reaction. Reasons that the oxidation potential of **2l** ($E^{\circ\prime}_{0/+} = +0.61$ V; CH_3CN) is 0.22 V higher than in the parent compound **2k** are not easy to identify unequivocally, but two possibilities come readily to mind: Introducing a third positive charge into **2l** and generating a trication is certainly disfavored for electrostatic reasons. However, a second point must also be taken into consideration. Methylation of **2k** reduces the Lewis basicity of the pyrazolyl substituent and thus further polarizes the exocyclic B−N bond, thereby decreasing the electron density at the boron atoms. This effect has to be distinguished from the electrostatic argument, because it would also be operative if the methylium cations were replaced by the uncharged BH_3 electrophile. An even higher oxidation potential as for the dication **2l** is observed when all pyrazolyl rings of **2k** are substituted with CF_3 groups in positions 3 and 5 (**2m**, $E^{\circ\prime}_{0/+} = +0.67$ V; CH_3CN). This testifies to the large extent of transmission of inductive effects along the pyrazabole framework. Similar arguments as outlined for the different amine substituents hold for R = OEt and Br. The electronegativity of oxygen is higher compared to nitrogen, and its π-donating ability is intermediate between that of pyrrolidine and pyrazole. Hence, in CH_3CN the redox potential of **2h** is 0.05 V [CH_2Cl_2, 0.11 V] more positive than in the case of the pyrrolidine compound **2n** but 0.13 V [CH_2Cl_2, 0.15 V] smaller than in the pyrazole derivative **2k**. Due to its large atomic radius, the π donation of bromine toward boron is negligible, and consequently **2a** exhibits the highest redox potential of all five compounds in the series ($E^{\circ\prime}_{0/+} = +0.40$ V; CH_3CN), even though its negative inductive effect is smaller than that of oxygen or nitrogen.

From the oxidation potentials of *ansa*-ferrocenes **2** with identical boron substituents, but different pyrazolyl bridges, some conclusions about the influence of ring substituents on the electron density at boron (and iron) can easily be drawn. For instance, a comparison of the formal electrode potentials of the couples **2c**/**2d**, **2h**/**2i**, and **2n**/**2p** indicates the electron-donating ability of the bridging heterocycles to follow the order triazole < indazole < pyrazole (Table 5). This is the expected result, since their pK_b values increase in the same order,[9] and it also fits to the interpretation of the X-ray crystal structure analyses discussed above. Switching from pyrazolyl to 3,5-dimethylpyrazolyl as bridging unit results in a decrease of the redox potential of 0.20 V (CH_3CN; redox couple **2a,b**), while electron-withdrawing CF_3 substituents lead to changes in the opposite direction (**2c,g**, $\Delta(E^{\circ\prime}_{0/+}) = 0.30$ V (CH_3CN)). Similar to the trifluoromethyl groups, which can be regarded as genuine σ acceptors, ester substituents, which are both σ *and* π acceptors, make the iron atom significantly harder to oxidize (**2c,f**, $\Delta(E^{\circ\prime}_{0/+}) = 0.13$ V (CH_3CN); **2h,j**, $\Delta(E^{\circ\prime}_{0/+}) = 0.14$ V (CH_3CN)).

A point of further interest lies in the fact that switching from the ferrocenophane to the open-chain species seems to be a process which does not involve important variations in the charge density of the boron center, as it goes from the four-coordinate to the three-coordinate state. In CH_3CN solution, the redox potentials of the iron centers change by not more than 0.07 V [CH_2Cl_2, 0.16 V] upon proceeding from **2c** to **2n** and further to the already air-sensitive **2p**, even though

Table 6. Peak Potential Values (in V) for the Oxidation and Reduction Processes Exhibited by Open-Chain Complexes 2q,r in CH_2Cl_2 Solution

2	$E_{p0/+}$[a]	$E_{p0/2-}$[a]
q	+0.31	−1.20
r	+0.33	−0.91

[a] Measured at 0.2 V s^{-1}.

significant structural alterations are obvious in their crystal structures (see above). Moreover, the rather small peak potentials of the irreversible oxidation of open-chain **2q,r** (**2q**, $E_{p0/+} = +0.31$ V (CH_2Cl_2); **2r**, $E_{p0/+} = +0.33$ V (CH_2Cl_2)), which will be discussed below, indicate the electron density at iron and boron to be not much different from that in the *ansa*-bridged derivatives.

Further to their ferrocene-centered oxidations, complexes **2b**,**n** display irreversible anodic processes at high potential values (**2b**, $E_p = +0.8$ and +1.0 V; **2n**, $E_p = +1.1$ and +1.3 V), which could be in principle assigned to the oxidation of the pyrazabole bridge.[26] However, the fact that **2d** with its extended π system in the *ansa*-bridge does not show such processes suggests their simple assignment to the oxidation of the boron substituents bromine (**2b**) and pyrrolidine (**2n**).

The results obtained so far from electrochemical measurements on ferrocene derivatives[27] suggest an application of ferrocenylboranes as Lewis acidic centers with electrochemically switchable Lewis acidity. It is well-known that ferrocenes bearing electron-withdrawing substituents are harder to oxidize than ferrocene itself. The half-wave oxidation potential of dihydroxyborylferrocene ($FcB(OH)_2$), for example, is +0.06 V relative the FcH/FcH^+ couple in aqueous solution. However, when Lewis bases like the fluoride anion are added to a solution of $FcB(OH)_2$, a gradual shift by 60 mV toward more negative values is observed for a 10-fold increase of fluoride ion concentration.[28] Given the fact that a direct iron-to-boron electron donation has been established for compounds $FcBR_2$ both by X-ray crystal structure determination (R = Br) and by density functional calculations (R = H),[29] it can be expected that oxidation of the iron atom of borylferrocenes leads to a pronounced increase in the Lewis acidity of the boron substituent. Apart from our general interest in redox-active Lewis acids, in the special case of compounds **A** oxidation of the ferrocene fragment may provide a possibility to influence their tendency to form Lewis acid−base pairs and hence to favor or disfavor *ansa*-bridge formation (i.e. to shift the equilibrium outlined in Figure 1). We have therefore tried to find out whether Fe oxidation in open-chain **2q,r** may be an irreversible process causing *ansa*-bridge formation. Indeed, both complexes exhibit a ferrocene centered one-electron oxidation coupled to chemical complications (Table 6), but cyclic voltammetry performed on their exhaustively oxidized solutions does not afford the typical well-shaped profiles discussed for *ansa*-bridged complexes. These compounds also display a hard-to-

(26) Nöth, H.; Winterstein, W.; Kaim, W.; Bock, H. *Chem. Ber.* **1979**, *112*, 2494−2502.
(27) Zanello, P. In *Ferrocenes*; Togni, A., Hayashi, T., Eds.; VCH Verlagsgesellschaft mbH: Weinheim, Germany, 1995.
(28) Dusemund, C.; Sandanayake, K. R. A. S.; Shinkai, S. *J. Chem. Soc., Chem. Commun.* **1995**, 333−334.
(29) Appel, A.; Jäkle, F.; Priermeier, T.; Schmid, R.; Wagner, M. *Organometallics* **1996**, *15*, 1188−1194.

assign two-electron reduction step at $E_p(0/2-) = -1.20$ V (**2q**) and $E_p(0/2-) = -0.91$ V (**2r**), which in its turn is complicated by subsequent chemical reactions.

Conclusion

We have demonstrated that the stability of ferrocenophanes **2** with pyrazabole bridges depends to a large extent on the substitution pattern of boron and pyrazole. Strongly π-donating substituents at boron (e.g. pyrrolidine) result in a weakening of the interannular bridge. Strongly electron-withdrawing groups at the pyrazole rings also lead to a destabilization of the pyrazabole dimer. This is true for ester substituents with their large negative mesomeric effect, as well as for CF_3 moieties, which are merely σ acceptors. The derivative **2p** with a pyrrolidine group ligated to boron and bridging triazolyl rings is particularly interesting, because it provides some evidence for thermal *ansa*-bridge opening at high temperatures (boiling di-*n*-butyl ether). Moreover, this molecule can also be switched into the open-chain state with the help of Lewis acidic additives, i.e. by methylating the triazolyl nitrogen atoms N4.

Electrochemistry proved that the *ansa*-bridged derivatives of **2** undergo reversibly the Fe(II)/Fe(III) redox change, whereas the oxidation process of open-chain **2q,r** is accompanied by degradation of their oxidized congeners. The formal electrode potentials of *ansa*-**2** give a qualitative picture of the electronic effects exerted by the wide variety of substituents attached to boron or to the pyrazolyl moieties. Remarkably large differences in the $E^{\circ\prime}_{0/+}$ values, which range from 0.15 V (**2c**) to 0.67 V (**2m**), are observed, thus showing the electronic effects of the substituents to be transmitted to a great degree along the pyrazabole framework. Given this background, the differences in the redox potentials of the series **2c,n,p,q(r)** are remarkably small, indicating the process of gradual *ansa*-bridge weakening (and finally opening) to occur without major alterations of the charge density at boron. The expected electron deficiency at the four-coordinate boron atoms caused by the increased σ bond polarity upon going from **2c** to **2n** is probably offset by negative hyperconjugation. Further evidence for this interpretation stems from a comparison of the X-ray crystal structure investigation of **2c,n,p**, where a gradual increase of the endocyclic B−N bonds, together with unusually short exocyclic B−N links (**2n,p**) and a severe flattening of the pyrrolidine nitrogen atoms, is observed. This finding again is in accord with the assumption of pyrrolidine π donation into the antibonding B−N σ orbitals of the pyrazabole bridge.

Experimental Section

General Considerations. All reactions and manipulations of air-sensitive compounds were carried out in dry, oxygen-free argon using standard Schlenkware or in an argon-filled drybox. Solvents were freshly distilled under N_2 from Na/K alloy−benzophenone (toluene, hexane, Et_2O, *n*-Bu_2O, THF) or from CaH_2 (CH_2Cl_2, CH_3CN) prior to use. Instruments: IR, solvent toluene or CH_2Cl_2 (organic and organometallic compounds), Perkin-Elmer 1650 FT-IR; NMR, Jeol JMN-GX 400, Bruker DPX 400, and Bruker MSL 300 (solid-state NMR); MS (CI, FAB, FD mode): Finnigan MAT 90. ^{11}B NMR spectra are reported relative to external $BF_3{\cdot}Et_2O$. ^{19}F NMR spectra were run using $F_3CC_6H_5$ (0.05% solution in $CDCl_3$) as external reference; the chemical shifts are reported relative to CCl_3F. The solid-state ^{13}C NMR spectrum was run using the MAS technique; adamantane was employed as external reference. In the case of paramagnetic **2c**$^+$, the chemical shifts δ^{exp} relative to internal CD_3CN are given. Unless stated otherwise, all NMR spectra were run at ambient temperature. Abbreviations: s = singlet; d = doublet; tr = triplet; vtr = virtual triplet; q = quartet; sept = septet; vsept = virtual septet; br = broad; mult = multiplet; n.r. = multiplet expected in the ^{1}H NMR spectrum, but not resolved; pz = pyrazolyl; ind = indazolyl; tz = triazolyl. The numbering of the *ansa*-bridges in compounds **2** follows the common numbering scheme for the parent heterocycles. Elemental analyses: Microanalytical laboratory of the Technische Universität München.

The compounds **1a,b**[30] and **1c,d**[3] were synthesized according to literature procedures.

Synthesis of 2c$^+$. Solid **2c** (0.05 g, 0.14 mmol) was mixed in a Schlenk tube with excess $AgBF_4$ (0.10 g, 0.51 mmol), and the mixture was treated with THF (20 mL) at ambient temperature and stirred for 1 h. The resulting blue suspension was evaporated *in vacuo* and the gray-blue solid residue extracted with CH_2Cl_2. After filtration the resulting blue solution was layered with hexane and stored at 5 °C, whereupon dark blue X-ray-quality crystals formed in almost quantitative yield.

^{11}B NMR (128.3 MHz, CD_3CN, 30 °C): δ^{exp} −23 ($h_{1/2}$ = 150 Hz, Cp−B), −3 ($h_{1/2}$ = 25 Hz, BF_4^-). ^{1}H NMR (400.0 MHz, CD_3CN, 30 °C): δ^{exp} −4.0 (br, 2H, pz-H_4), −0.5 (br, 4H, pz-$H_{3,5}$), 4.3 (br, 6H, Me), 29.3 , 38.0 (2 × very br, 2 × 4H, C_5H_4). ^{13}C NMR (100.5 MHz, CD_3CN, 30 °C, proton-coupled): δ^{exp} −84.8 (br, Me), 92.6 (d, J(CH) = 185 Hz, pz-C_4), 117.4 (d, J(CH) = 185 Hz, pz-$C_{3,5}$), 243.1 (br, C_5H_4), 333.9 (br, C_5H_4-*ipso*), 383.8 (br, C_5H_4). Anal. Calcd for $C_{18}H_{20}B_3F_4FeN_4$ (456.66): C, 47.34; H, 4.42; N, 12.26. Found: C, 47.61; H, 4.13; N, 12.37.

Synthesis of 2d. A toluene solution of **1b** (0.92 g, 2.33 mmol, −40 °C) was added dropwise with stirring to a solution of indazole (0.55 g, 4.65 mmol) in 120 mL of toluene at −40 °C. Neat NEt_3 (0.47 g, 4.65 mmol) was added, and the reaction mixture was warmed to ambient temperature and stirred for 12 h. After filtration and evaporation of the solvent *in vacuo*, the crude product was purified by passing it down a short chromatography column (silica gel, ambient temperature) using 2/1 toluene/hexane as eluent. All material to elute was collected, the solution evaporated *in vacuo*, and the resulting microcrystalline solid recrystallized from di-*n*-butyl ether. Yield: 0.65 g (59%); *rac*:*meso* = 3:7. A small proportion of **2d** (*rac*/*meso*) was redissolved in toluene, and the solution was slowly evaporated by placing the test tube at 20 °C in a desiccator filled with paraffine pellets. The first crystals formed were found to be pure *meso*-**2d** (NMR spectroscopy; X-ray crystal structure determination).

***rac*-2d.** ^{11}B NMR (128.3 MHz, $CDCl_3$): δ 1.3 ($h_{1/2}$ = 200 Hz). ^{1}H NMR (400.0 MHz, $CDCl_3$): δ 1.11 (s, 6H, Me), 3.18, 3.20, 3.88, 3.91 (4 × n.r., 4 × 2H, C_5H_4), 7.26 (vtr, 2H, J(HH) = 8.0 Hz, ind-H_5), 7.50 (vtr, 2H, J(HH) = 8.0 Hz, ind-H_6), 7.86 (d, 2H, J(HH) = 8.0 Hz, ind-H_4), 8.11 (d, 2H, J(HH) = 8.0 Hz, ind-H_7), 8.57 (s, 2H, ind-H_3). ^{13}C NMR (100.5 MHz, $CDCl_3$): δ 11 (br, Me), 69.1, 69.3, 69.5, 70.1 (C_5H_4), n.o. (C_5H_4-*ipso*), 114.5 (ind-C_7), 121.6 (ind-C_4), 121.6 (ind-C_9), 122.2 (ind-C_5), 129.0 (ind-C_6), 129.2 (ind-C_3), 143.9 (ind-C_8).

***meso*-2d.** ^{11}B NMR (128.3 MHz, $CDCl_3$): δ 1.3 ($h_{1/2}$ = 500 Hz). ^{1}H NMR (400.0 MHz, $CDCl_3$): δ 0.87, 1.33 (2 × s, 2 × 3H, Me), 3.16, 3.21, 3.88, 3.91 (4 × n.r., 4 × 2H, C_5H_4), 7.26 (vtr, 2H, J(HH) = 8.0 Hz, ind-H_5), 7.50 (vtr, 2H, J(HH) = 8.0 Hz, ind-H_6), 7.86 (d, 2H, J(HH) = 8.0 Hz, ind-H_4), 8.22 (d, 2H, J(HH) = 8.0 Hz, ind-H_7), 8.45 (s, 2H, ind-H_3). ^{13}C NMR (100.5 MHz, $CDCl_3$): δ 10 (br, Me), 69.1, 69.3, 69.3, 70.3 (C_5H_4), n.o. (C_5H_4-*ipso*), 115.3 (ind-C_7), 121.5 (ind-C_4), 122.0 (ind-C_9), 122.2 (ind-C_5), 128.8 (ind-C_6), 129.0 (ind-C_3), 144.1 (ind-C_8). CI-

(30) Ruf, W.; Renk, T.; Siebert, W. *Z. Naturforsch.* **1976**, *31b*, 1028−1034.

MS: *m/z* 470 [(M^+); 100%], 455 [($M^+ - CH_3$); 5%]. Anal. Calcd for $C_{26}H_{24}B_2FeN_4$ (469.97): C, 66.45; H, 5.16; N, 11.92. Found: C, 66.49; H, 5.41; N, 11.87.

Synthesis of 2g. A slurry of lithium 3,5-bis(trifluoromethyl)pyrazolide (0.41 g, 1.96 mmol; generated from 3,5-bis(trifluoromethyl)pyrazole and *n*-butyllithium in hexane) in 25 mL of toluene was cooled to −30 °C. A solution of **1b** (0.37 g, 0.93 mmol) was added dropwise with stirring; the mixture was then allowed to warm to ambient temperature, stirred for 12 h, and filtered through a frit. The solvent was removed from the filtrate under reduced pressure to yield an orange solid. Volatile material was sublimed off (60 °C, 10^{-2} Torr) and the remaining crude **2g** recrystallized from toluene/hexane (1:10). Yield: 0.40 g (67%).

^{11}B NMR (128.3 MHz, $CDCl_3$): δ 5.3 ($h_{1/2}$ = 300 Hz). ^{1}H NMR (400.0 MHz, C_6D_6): δ 1.00 (s, 6H, Me), 3.12, 4.02 (2 × n.r., 2 × 4H, C_5H_4), 6.80 (s, 2H, pz-H_4). ^{13}C NMR (100.5 MHz, C_6D_6): δ 7.4 (br, CH_3), 69.6, 70.9 (C_5H_4), 78.3 (br, C_5H_4-*ipso*), 114.0 (br, pz-C_4), 119.5 (q, J(CF) = 271 Hz, CF_3), 140.0 (q, J(CF) = 42 Hz, pz-$C_{3,5}$). ^{19}F NMR (376.5 MHz, C_6D_6): δ −54.2 (CF_3). CI-MS: *m/z* 642 [(M^+); 15%]. Anal. Calcd for $C_{22}H_{16}B_2F_{12}FeN_4$ (641.84): C, 41.17; H, 2.51; F, 35.52; N, 8.73. Found: C, 41.50; H, 2.65; F, 35.18; N, 8.96.

Synthesis of 2i. A toluene solution of **1a** (1.46 g, 2.78 mmol) was treated at 0 °C with neat diethyl ether (0.41 g, 5.54 mmol). The mixture was stirred for 5 days at ambient temperature, all volatiles were removed *in vacuo*, and the resulting **1c** was used without further purification. **1c** was redissolved in 50 mL of toluene and cooled to −78 °C, and a solution of triazole (0.37 g, 5.36 mmol) in 100 mL of toluene was added slowly with stirring. After the addition of neat NEt_3 (0.55 g, 5.44 mmol), the reaction mixture was warmed to ambient temperature, stirred for 12 h, filtered, and evaporated *in vacuo*. The crude product was recrystallized from toluene/hexane (1:3). Yield: 0.54 g (45%).

^{11}B NMR (128.3 MHz, $CDCl_3$): δ 5.0 ($h_{1/2}$ = 200 Hz). ^{1}H NMR (400.0 MHz, $CDCl_3$): δ 1.23 (tr, 6H, J(HH) = 7.0 Hz, OCH_2CH_3), 3.42 (vtr, 4H, J(HH) = 1.5 Hz, C_5H_4), 3.71 (q, 4H, J(HH) = 7.0 Hz, OCH_2CH_3), 4.13 (vtr, 4H, J(HH) = 1.5 Hz, C_5H_4), 8.45 (s, 4H, tz-$H_{3,5}$). ^{13}C NMR (100.5 MHz, $CDCl_3$): δ 18.3 (OCH_2CH_3), 61.1 (OCH_2CH_3), 70.7, 71.3 (C_5H_4), n.o. (C_5H_4-*ipso*), 147.2 (tz-$C_{3,5}$). CI-MS: *m/z* 432 [(M^+); 50%], 387 [($M^+ - OC_2H_5$); 100%], 364 [($M^+ - N_3C_2H_2$); 20%]. Anal. Calcd for $C_{18}H_{22}B_2FeN_6O_2$ (431.88): C, 50.06; H, 5.13; N, 19.46. Found: C, 49.88; H, 4.94; N, 19.20.

Synthesis of 2l. A solution of **2k** (0.40 g, 0.84 mmol) in 15 mL of CH_2Cl_2 was added dropwise at −78 °C to a slurry of $Me_3O^+BF_4^-$ (0.25 g, 1.69 mmol) in 30 mL of CH_2Cl_2. Upon warming a clear solution was observed at 0 °C, which later became cloudy again. The mixture was stirred at ambient temperature for 12 h. The insoluble yellow material was collected on a frit, extracted with 10 mL of CH_2Cl_2, and dried *in vacuo*. The crude **2l** was recrystallized at −25 °C from toluene/CH_3CN (2:1). Yield: 0.49 g (76%). Two stable rotamers were obtained (rotamer 1:rotamer 2 = 9:1).

^{11}B NMR (128.3 MHz, CD_3CN): δ −1.5 ($h_{1/2}$ = 15 Hz; BF_4^-), 1.0 ($h_{1/2}$ = 150 Hz; Cp−B).

Rotamer Spectral Data. Rotamer 1: ^{1}H NMR (400.0 MHz, CD_3CN) δ 3.43 (s, 6H, Me), 3.58 (vtr, 4H, J(HH) = 1.8 Hz, C_5H_4), 4.30−4.35 (mult, 4H, C_5H_4), 6.81, 6.93 (tr, vtr, 2 × 2H, endo/exo-pz-H_4), 7.93 (d, 4H, J(HH) = 2.4 Hz, endo-pz-$H_{3,5}$), 8.00, 8.30 (2 × d, 2 × 2H, J(HH) = 2.7 Hz, exo-pz-$H_{3,5}$). Rotamer 2: ^{1}H NMR (400.0 MHz, CD_3CN) δ 3.42 (s, 3H, Me), 3.61, 3.63 (2 × vtr, 2 × 2H, J(HH) = 1.8 Hz, C_5H_4), 3.73 (s, 3H, Me), 4.30−4.35 (mult, 2H, C_5H_4), 4.38 (vtr, 2H, J(HH) = 1.8 Hz, C_5H_4), 6.79−6.85 (mult, 2H, exo-pz-H_4) 6.87 (vtr, 2H, J(HH) = 2.4 Hz, endo-pz-H_4), 7.84, 7.95 (2 × d, 2 × 2H, J(HH) = 2.4 Hz, endo-pz-$H_{3,5}$), 8.02, 8.19, 8.26 (3 × d, 2H, 2 × 1H, J(HH) = 2.4 Hz, exo-pz-$H_{3,5}$). Rotamer 1: ^{13}C NMR (100.5 MHz, CD_3CN) δ 40.3 (Me), 73.6, 73.7 (C_5H_4), n.o. (C_5H_4-*ipso*), 109.4, 111.3 (endo/exo-pz-C_4), 139.8 (endo-pz-$C_{3,5}$), 144.7, 146.3 (exo-pz-$C_{3,5}$). Rotamer 2: Satisfactory ^{13}C NMR spectra were not obtained, due to the small amount of rotamer 2 present in the mixture. FD-MS: *m/z* 591 [($M - BF_4^-$)$^+$; 100%]. Anal. Calcd for $C_{24}H_{26}B_4F_8FeN_8$ (677.60)·CH_3CN(41.05)·0.5C_7H_8 (92.14): C, 46.33; H, 4.35; F, 19.87; N, 16.48. Found: C, 46.39; H, 4.26; F, 19.88; N, 16.80 (the amount of solvents present in crystalline **2l** was also confirmed by ^{1}H NMR spectroscopy in [D_6]acetone solution).

Synthesis of 2m. 3,5-Bis(trifluoromethyl)pyrazole (0.77 g, 3.77 mmol) was dissolved in 40 mL of toluene, cooled to −78 °C, and treated with a solution of **1a** (0.48 g, 0.92 mmol) in 15 mL of toluene. After 5 min, neat NEt_3 (0.38 g, 3.77 mmol) was added, and the mixture was warmed to ambient temperature and stirred for 12 h. After filtration, the solvent was removed from the filtrate under reduced pressure. The crude product was extracted with hexane (2 × 10 mL) and recrystallized from toluene/hexane (1:5) at −25 °C to give orange **2m**. Yield: 0.81 g (86%). Two stable rotamers were obtained, which could not be separated from each other. Therefore, the NMR spectra of the mixture are given (rotamer 1:rotamer 2 = 4:5).

^{11}B NMR (128.3 MHz, C_6D_6): δ 4.6 ($h_{1/2}$ = 300 Hz). ^{1}H NMR (400.0 MHz, C_6D_6): δ 3.18, 3.28, 3.29 (3 × n.r., 2 × 2H, 4H, C_5H_4), 3.84, 3.91 (2 × vtr, 2H, 4H, J(HH) = 1.8 Hz, C_5H_4), 4.00 (n.r., 2H, C_5H_4), 6.34, 6.38, 6.67, 6.68, 6.72 (5 × s, 2 × 2H, 2 × 1H, 2H, pz-H_4). ^{13}C NMR (100.5 MHz, $CDCl_3$): δ 72.0, 72.2, 72.5 (C_5H_4), 73.1 (q, J(CF) = 3.7 Hz, C_5H_4) 73.4, 73.7 (2 × mult, C_5H_4), n.o. (C_5H_4-*ipso*), 109.9, 110.4 (2 × br, pz-C_4), 114.2, 114.5 (sept, vsept, J(CF) = 4.6 Hz, pz-C_4), 117.3, 117.3, 117.4, 118.8, 119.4, 120.3, 120.3, 120.5 (8 × q, J(CF) = 270 Hz, CF_3), 140.6, 143.0, 146.0 (3 × q, J(CF) = 41 Hz, pz-$C_{3,5}$), n.o. (other pz-$C_{3,5}$). ^{19}F NMR (376.5 MHz, $CDCl_3$): rotamer 1, δ −63.9 (s, 6F, exo-CF_3), −59.7 (q, 12F, J(FF) = 10 Hz, endo-CF_3), −56.8 (sept, 6F, J(FF) = 10 Hz, exo-CF_3); rotamer 2, δ -65.0, −63.9, −61.3 (3 × s, 3 × 3F, exo-CF_3), −60.2 (q, 6F, J(FF) = 10 Hz, endo-CF_3), −59.1 (s, 6F, endo-CF_3), −57.1 (sept, 3F, J(FF) = 10 Hz, exo-CF_3). CI-MS: *m/z* 1018 [(M^-); 100%]. Anal. Calcd for $C_{30}H_{12}B_2F_{24}FeN_8$ (1017.90): C, 35.40; H, 1.19; F, 44.79; N, 11.01. Found: C, 36.04; H, 1.61; F, 43.52; N, 10.84.

Synthesis of 2o. A solution of indazole (0.24 g, 2.03 mmol) in 40 mL of toluene was added dropwise to a toluene solution of **1d** (0.50 g, 0.99 mmol) at −20 °C. Neat NEt_3 (0.20 g, 1.98 mmol) was added, and the reaction mixture was warmed to ambient temperature and stirred for 12 h. After filtration and evaporation of the solvent *in vacuo*, the crude product was recrystallized from toluene/hexane (1:10) to give **2o** as an orange microcrystalline solid. Yield: 0.49 g (85%); *rac*:*meso* = 1:1.

***rac*/*meso* Data.** ^{11}B NMR (128.3 MHz, $CDCl_3$): δ 3.0 ($h_{1/2}$ = 500 Hz). ^{1}H NMR (400.0 MHz, $CDCl_3$): δ 1.91 (mult, 14H, NCH_2CH_2), 2.02 (mult, 2H, NCH_2CH_2), 2.77, 2.83, 2.88, 3.06 (tr, 2 × mult, br, 3 × 2H, 4H, NCH_2CH_2), 3.15 (mult, 8H, C_5H_4), 3.27, 3.30, 3.45 (2 × mult, tr, 3 × 2H, NCH_2CH_2), 3.86 (mult, 8H, C_5H_4), 7.25 (mult, 4H, ind-H_5), 7.50 (mult, 4H, ind-H_6), 7.85 (d, 4H, ind-H_4), 7.98 (mult, 4H, ind-H_7), 8.32, 8.37 (2 × s, 2 × 2H, ind-H_3). ^{13}C NMR (100.5 MHz, $CDCl_3$): δ 27.0, 27.1, 27.2, 27.3 (NCH_2CH_2), 46.5, 47.0, 49.7, 49.9 (NCH_2CH_2), 68.5, 68.6, 68.7, 68.9, 70.3, 70.6, 71.0, 71.3 (C_5H_4), n.o. (C_5H_4-*ipso*), 115.1, 115.2 (ind-C_7), 121.1, 121.1, 121.2, 121.2, 121.9, 122.0 (ind-C_4/C_5/C_9), 128.7, 128.7, 128.8, 128.9 (ind-C_3/C_6), 143.8, 144.0 (ind-C_8). Anal. Calcd for $C_{32}H_{34}B_2FeN_6$ (580.14): C, 66.25; H, 5.91; N, 14.49. Found: C, 66.59; H, 6.15; N, 14.44.

Synthesis of 2p,s. A toluene solution of **1d** (0.45 g, 0.89 mmol) was treated at −78 °C with a solution of triazole (0.12 g, 1.74 mmol) in 40 mL of toluene. Neat NEt_3 (0.18 g, 1.78 mmol) was added, and the reaction mixture was warmed to ambient temperature and stirred for 12 h. After filtration and evaporation of the solvent *in vacuo*, the crude product was extracted with hexane and recrystallized from toluene/hexane (1:2) at −25 °C. Yield: 0.26 g (61%). When crude **2p** is recrystallized from boiling di-*n*-butyl ether, the crystalline material was found to contain exclusively **2s** as the result of a substituent exchange reaction.

2p. ^{11}B NMR (128.3 MHz, $CDCl_3$): δ 2.7 ($h_{1/2}$ = 200 Hz). ^{1}H NMR (400.0 MHz, $CDCl_3$): δ 1.78 (mult, 8H, NCH_2CH_2), 2.87 (mult, 8H, NCH_2CH_2), 3.28, 4.03 (2 × vtr, 2 × 4H, J(HH) = 1.8 Hz, C_5H_4), 8.30 (s, 4H, tz-$H_{3,5}$). ^{13}C NMR (100.5 MHz, $CDCl_3$): δ 26.9 (NCH_2CH_2), 48.0 (NCH_2CH_2), 69.7, 70.7 (C_5H_4), n.o. (C_5H_4-*ipso*), 147.6 (tz-$C_{3,5}$). CI-MS: m/z 482 [(M^+); 100%], 412 [($M^+ - NC_4H_8$); 80%]. Anal. Calcd for $C_{22}H_{28}B_2FeN_8$ (481.99): C, 54.82; H, 5.86; N, 23.25. Found: C, 55.10; H, 5.95; N, 23.04.

2s. ^{11}B NMR (128.3 MHz, $CDCl_3$): δ 0.6 ($h_{1/2}$ = 200 Hz), 3.8 ($h_{1/2}$ = 300 Hz). ^{1}H NMR (400.0 MHz, $CDCl_3$): δ 1.82 (mult, 4H, NCH_2CH_2), 2.91 (mult, 4H, NCH_2CH_2), 3.42, 3.47, 4.16, 4.23 (4 × vtr, 4 × 2H, J(HH) = 1.5 Hz, C_5H_4), 7.83 (s, 2H, endo-tz-$H_{3,5}$), 8.17 (s, 1H, exo-tz-$H_{3,5}$), 8.23 (s, 1H, exo-tz-$H_{3,5}$), 8.38 (s, 2H, endo-tz-$H_{3,5}$). ^{13}C NMR (100.5 MHz, $CDCl_3$): δ 27.0 (NCH_2CH_2), 48.1 (NCH_2CH_2), 70.9, 71.1, 71.3, 71.5 (C_5H_4), n.o. (C_5H_4-*ipso*), 147.7, 148.4 (endo-tz-$C_{3,5}$), 151.5, 155.2 (exo-tz-C3,5). CI-MS: m/z 480 [(M^+); 100%], 412 [($M^+ - N_3C_2H_2$); 80%]. Anal. Calcd for $C_{20}H_{22}B_2FeN_{10}$ (479.93)·0.5*n*-Bu_2O (130.09): C, 52.89; H, 5.73; N, 25.70. Found: C, 52.86; H, 5.99; N, 25.51.

Solid-State ^{13}C NMR Spectrum of 2q. The synthesis and the NMR spectra of **2q** in solution have already been described.[3]

^{13}C NMR (75.5 MHz, CP/MAS): δ 13.9, 16.0 (2 × br, $COOCH_2CH_3$), 26.6 (br, NCH_2CH_2), 49.4 (NCH_2CH_2), 62.5 ($COOCH_2CH_3$), 65.9, 72.6, 76.9 (3 × br, C_5H_4), 121.7 (pz-C_4), 134.7 (pz-$C_{3,5}$), 143.3 (pz-$C_{3,5}$), 159.7, 161.9, 164.0 (CO).

Synthesis of 2r. A toluene solution of **1d** (0.57 g, 1.13 mmol) was treated at −78 °C with a solution of 3,5-bis-(trifluoromethyl)pyrazole (0.46 g, 2.25 mmol) in 20 mL of toluene. Neat NEt_3 (0.23 g, 2.26 mmol) was added, and the reaction mixture was warmed to ambient temperature and stirred for 12 h. After filtration and evaporation of the solvent *in vacuo*, the crude product was recrystallized from toluene/hexane (1:15) at −78 °C. Yield: 0.62 g (73%).

^{11}B NMR (128.3 MHz, $CDCl_3$): δ 33.7 ($h_{1/2}$ = 400 Hz). ^{1}H NMR (400.0 MHz, $CDCl_3$): δ 1.75, 1.95 (2 × mult, 2 × 4H, NCH_2CH_2), 2.89, 3.11 (2 × mult, 2 × 2H, NCH_2CH_2), 3.45−3.67 (mult, 4H, NCH_2CH_2, 2H, C_5H_4), 4.37, 4.49, 4.50, 4.52, 4.54, 4.66 (6 × vtr, 6 × 1H, J(HH) = 1.2 Hz, C_5H_4), 6.91, 6.93 (2 × s, 2 × 1H, pz-H_4). ^{13}C NMR (100.5 MHz, $CDCl_3$): δ 25.4, 25.5, 26.6, 26.7 (NCH_2CH_2), 48.3, 48.4, 48.6, 48.6 (NCH_2CH_2), 73.7, 73.7, 74.5, 74.6, 74.6, 75.0, 75.4, 76.0 (C_5H_4), n.o. (C_5H_4-*ipso*), 104.9 (pz-C_4), 119.7, 121.0 (2 × q, J(CF) = 269 Hz, CF_3), 136.2, 136.4 (2 × q, J(CF) = 40 Hz, pz-C_3), 144.4 (q, J(CF) = 38 Hz, pz-C_5). ^{19}F NMR (376.5 MHz, $CDCl_3$): δ −63.0, −63.0, −60.3, −60.2 (CF_3). Anal. Calcd for $C_{28}H_{26}B_2F_{12}FeN_6$ (752.00): C, 44.72; H, 3.49; F, 30.32; N, 11.18. Found: C, 44.31; H, 3.35; F, 29.93; N, 10.99.

Generation of 3. A suspension of $Me_3O^+BF_4^-$ (0.14 g, 0.95 mmol) in CH_2Cl_2 was cooled to −78 °C and treated with a CH_2Cl_2 solution of **2i** (0.20 g, 0.46 mmol). The cloudy yellow mixture was allowed to warm to ambient temperature and stirred overnight. A small amount of insoluble material was collected on a frit (G4) and the orange filtrate evaporated *in vacuo* to give an orange oily residue. This product was treated with 30 mL of hexane and the mixture filtered from a white solid precipitate. The solvent was removed from the filtrate *in vacuo*. The remaining orange oil was still contaminated with a small amount of unknown, probably ferrocene-containing, species and identified as **3** by means of NMR spectroscopy.

^{11}B NMR (128.3 MHz, $CDCl_3$): δ 28.3 ($h_{1/2}$ = 300 Hz). ^{1}H NMR (400.0 MHz, $CDCl_3$): δ 1.32 (tr, 6H, J(HH) = 7.0 Hz, OCH_2CH_3), 4.09 (q, 4H, J(HH) = 7.0 Hz, OCH_2CH_3), 4.39 (br, 8H, C_5H_4). ^{13}C NMR (100.5 MHz, $CDCl_3$): δ 17.3 (OCH_2CH_3), 59.3 (d, J(CF) = 10.7 Hz, OCH_2CH_3), 73.0 (C_5H_4), 74.3 (d, J(CF) = 3.9 Hz, C_5H_4). Due to the oily nature of the product a satisfactory elemental analysis was not obtained.

X-ray Single-Cystal Structure Determination of 2c$^+$.[12] Suitable crystals were grown from CH_2Cl_2/hexane (1:1) at 5 °C. Crystal data together with details of the data collection and structure refinement are listed in Table 1. Preliminary examination and data collection were carried out on an imaging plate diffraction system (IPDS; Stoe & Cie) equipped with a rotating anode (Enraf Nonius FR591; 50 kV; 80 mA; 4.0 kW) and graphite-monochromated MoK$\bar{\alpha}$ radiation. The data collection was performed at 193 ± 1 K within the Θ-range of 4.5° < Θ < 26.0° with an exposure time of 2 min per image (rotating scan modus from φ = 0° to 360° with $\Delta\varphi$ = 1°). A total number of 45 311 reflections were collected, from which a sum of 12 770 independent reflections remained and were used for all calculations. Data were corrected for Lorentz and polarization effects.[31] Corrections for intensity decay, absorption effects and extinction were not necessary and were not applied. The unit cell parameters were obtained by least squares refinements of 1973 reflections with the program Cell.[31,32] The structure was solved by the Patterson method and refined with standard difference Fourier techniques. All "heavy atoms" of the asymmetric unit were anisotropically refined, except for four disordered fluorine atoms of two BF_4^- anions. All hydrogen atoms were calculated in ideal positions (riding model). Full matrix least squares refinements were carried out by minimizing $\Sigma w(F_o^2 - F_c^2)^2$ with the SHELXL weighting scheme and stopped at shift/err < 0.005, with w$R2$ = 0.116 and $R1$ = 0.050 for all data (residual electron density +0.82, −0.53 e Å^{-3}). The correct polarity of the crystal is proved by refining Flack's parameter to 0.01(1). Neutral atom scattering factors for all atoms and anomalous dispersion corrections for the non-hydrogen atoms were taken from the ref 33. All calculations were performed on a DEC 3000 AXP workstation with the STRUX-V system,[34] including the programs PLATON-92,[35] PLUTON-92,[35] SHELXS-86,[36] and SHELXL-93.[37] Selected bond lengths and angles are given in Tables 2 and 3.

X-ray Single-Cystal Structure Determination of *meso*-2d.[12] Suitable crystals were grown from a toluene solution at ambient temperature. Crystal data together with details of the data collection and structure refinement are listed in Table 1. Preliminary examination and data collection were carried out on an automatic four-circle diffractometer (CAD4, Enraf Nonius) equipped with a sealed tube and graphite-monochromated MoK$\bar{\alpha}$ radiation. The data collection was performed at 193 ± 1 K within the Θ-range of 1.0° < Θ < 26.0°, using the ω-scan method, maximal acquisition time 60 s for a single reflection. A total number of 4520 reflections were collected, from which a sum of 4098 independent reflections remained and were used for all calculations. Data were corrected for Lorentz and polarization effects.[38] Corrections for intensity decay, absorption effects, and extinction were not necessary and were not applied. The unit cell parameters were obtained by least-squares refinements of 25 high-angle reflections.[38] The structure was solved by direct methods and refined with standard difference Fourier techniques. All "heavy atoms" of the asymmetric unit were anisotropically refined. All hydrogen atoms were located in difference Fourier maps and refined isotropically. Full-matrix least-squares refinements were carried out by minimizing $\Sigma w(F_o^2 - F_c^2)^2$ with the SHELXL weighting scheme and stopped at shift/err < 0.001, with w$R2$ = 0.077 and $R1$ = 0.031 for all data (residual electron density

(31) *IPDS Operating System Version 2.6*; STOE & CIE; GmbH: Darmstadt, Germany, 1995.
(32) Schütt, W.; Herdtweck, E.; Hahn, F.; Kreissl, F. R. *J. Organomet. Chem.* **1993**, *443*, C33−C36 and references cited therein.
(33) *International Tables for Crystallography*; Wilson, A. J. C., Ed.; Kluwer Academic Publishers: Dordrecht, The Netherlands, 1992; Vol. C, Tables 6.1.1.4 (pp 500−502), 4.2.6.8 (pp 219−222), 4.2.4.2 (pp 193−199).
(34) Artus, G.; Scherer, W.; Priermeier, T.; Herdtweck, E. *STRUX-V, A Program System to Handle X-ray Data*; TU München: Germany, 1994.
(35) Spek, A. L. *Acta Crystallogr.* **1990**, *A46*, C34.
(36) Sheldrick, G. M. *SHELXS-86: Program for Crystal Structure Solutions*; Universität Göttingen: Göttingen, Germany, 1986.
(37) Sheldrick, G. M. *J. Appl. Crystallogr.* **1993**, in press.
(38) Fair, C. K. *MolEN: An Interactive Intelligent System for Crystal Structure Analysis*; Enraf-Nonius: Delft, The Netherlands, 1990.

+0.30, −0.37 e Å^{-3}). Neutral atom scattering factors for all atoms and anomalous dispersion corrections for the non-hydrogen atoms were taken from the ref 33. All calculations were performed on a DEC 3000 AXP workstation with the STRUX-V system,[34] including the programs PLATON-92,[35] PLUTON-92,[35] SIR-92,[39] and SHELXL-93.[37] Selected bond lengths and angles are given in Tables 2 and 3.

X-ray Single-Cystal Structure Determination of 2n.[12] Suitable crystals were grown from di-*n*-dibutyl ether at −20 °C. Crystal data together with details of the data collection and structure refinement are listed in Table 1. Preliminary examination and data collection were carried out on an automatic four-circle diffractometer (CAD4, Enraf Nonius) equipped with a sealed tube and graphite monochromated MoK$\bar{\alpha}$ radiation. The data collection was performed at 193 ± 1 K within the Θ-range of 1.0° < Θ < 26.0°, using the ω-scan method, maximal acquisition time 60 s for a single reflection. A total number of 5280 reflections were collected, from which a sum of 4024 independent reflections remained and were used for all calculations. Data were corrected for Lorentz and polarization effects.[38] Corrections for intensity decay, absorption effects, and extinction were not necessary and were not applied. The unit cell parameters were obtained by least-squares refinements of 25 high-angle reflections.[38] The structure was solved by direct methods and refined with standard difference Fourier techniques. All "heavy atoms" of the asymmetric unit were anisotropically refined. All hydrogen atoms were located in difference Fourier maps and refined isotropically. Full-matrix least-squares refinements were carried out by minimizing $\Sigma w(F_o^2 - F_c^2)^2$ with the SHELXL weighting scheme and stopped at shift/err < 0.001, with w$R2$ = 0.089 and $R1$ = 0.049 for all data (residual electron density +0.29, −0.31 e Å^{-3}). Neutral atom scattering factors for all atoms and anomalous dispersion corrections for the non-hydrogen atoms were taken from the ref 33. All calculations were performed on a DEC 3000 AXP workstation with the STRUX-V system[34], including the programs PLATON-92,[35] PLUTON-92,[35] SIR-92,[39] and SHELXL-93.[37] Selected bond lengths and angles are given in Tables 2 and 3.

X-ray Single-Cystal Structure Determination of 2p.[12] Suitable crystals were grown from toluene/hexane (1:2) at −25 °C. Crystal data together with details of the data collection and structure refinement are listed in Table 1. Preliminary examination and data collection were carried out on an automatic four-circle diffractometer (CAD4, Enraf Nonius) equipped with a sealed tube and graphite-monochromated MoK$\bar{\alpha}$ radiation. The data collection was performed at 193 ± 1 K within the Θ-range of 1.0° < Θ < 26.0°, using the ω-scan method, maximal acquisition time 90 s for a single reflection. A total number of 4088 reflections were collected, from which a sum of 3918 independent reflections remained and were used for all calculations. Data were corrected for Lorentz and polarization effects.[38] Corrections for intensity decay, absorption effects, and extinction were not necessary and were not applied. The unit cell parameters were obtained by least-squares refinements of 25 high-angle reflections.[38] The structure was solved by the Patterson method and refined with standard difference Fourier techniques. All "heavy atoms" of the asymmetric unit were anisotropically refined, even in the disordered pyrrolidine unit. All hydrogen atoms were located in difference Fourier maps and refined isotropically. Those located at the disordered carbon atom C(63) were calculated in ideal positions (riding model). Full matrix least squares refinements were carried out by minimizing $\Sigma w(F_o^2 - F_c^2)^2$ with SHELXL weighting scheme and stopped at shift/err < 0.001, with w$R2$ = 0.094 and $R1$ = 0.050 for all data (residual electron density +0.43, −0.33 e Å^{-3}). Neutral atom scattering factors for all atoms and anomalous dispersion corrections for the non-hydrogen atoms were taken from the ref 33. All calculations were performed on a DEC 3000 AXP workstation with the STRUX-V system,[34] including the programs PLATON-92,[35] PLUTON-92,[35] SHELXS-86,[36] and SHELXL-93.[37] Selected bond lengths and angles are given in Tables 2 and 3.

Electrochemical Measurements. The materials and apparatus for electrochemistry have been described elsewhere.[40] Direct current voltammograms on a platinum electrode with periodical renewal of the diffusion layer (DCV) have been obtained as previously described;[41] the samples have been examined both in CH_2Cl_2 and CH_3CN solution containing $[NBu_4][PF_6]$ (0.2 mol·dm^{-3}) and $[NEt_4][ClO_4]$ (0.1 mol·dm^{-3}) as supporting electrolytes, respectively. All the potential values are reported relative to the saturated calomel electrode (SCE).

Acknowledgment. We are grateful to Prof. Dr. W. A. Herrmann (Technische Universität München) for his generous support, to Dipl.-Chem. H. Heise (Technische Universität München) for recording the solid-state NMR spectrum, and to Prof. Dr. A. Berndt (Universität Marburg) for helpful discussions. Financial funding by the "Bayerischer Forschungsverbund Katalyse" (FORKAT), the "Deutsche Forschungsgemeinschaft", and the "Fonds der Chemischen Industrie" is acknowledged. P.Z. gratefully acknowledges the financial support by MURST of Italy, and G.O. acknowledges the University of Siena (Siena, Italy) for a one-year scholarship.

Supporting Information Available: Tables of X-ray parameters, atomic coordinates and thermal parameters, and bond distances and angles (39 pages). Ordering information is given on any current masthead page.

OM960722S

(39) Altomare, A.; Cascarano, G.; Giacovazzo, C.; Guagliardi, A.; Burla, M. C.; Polidori, G.; Camalli, M. *SIR-92*; University of Bari: Bari, Italy, 1992.

(40) Togni, A.; Hobi, M.; Rihs, G.; Rist, G.; Albinati, A.; Zanello, P.; Zech, D.; Keller, H. *Organometallics* **1994**, *13*, 1224−1234.

(41) Zanello, P.; Bartocci, C.; Maldotti, A.; Traverso, O. *Polyhedron* **1983**, *2*, 791−795.